Detection of Protrusion on Curved Folded Surface In Colon Capsule Endoscopy

Miss. Neeta B.Bankhele[1], Prof. Rahul M. Mulajkar[2]

[1]PG Student ,JCOE, kuran, Pune, Maharashtra, India
[2]PG Head ,JCOE, kuran, Pune, Maharashtra, India

---***---

Abstract - *In this paper a new method is proposed for the detection of polyp candidate sites on the colon surface. It is based on the notion that polyp tissue growth introduces a local deformation of the colon surface. The method estimates the original 'undeformed' surface position by solving a nonlinear partial differential equation. Candidate sites are obtained by comparing the two surfaces. The method is assessed by a supervised classification, based on features obtained from the deformation field and the grey level CT image*

***Key Words*:** Biomedical Image processing, Polyp detection, Colorectal cancer, Capsule Endoscopy

1.INTRODUCTION

CT colonography is a modern, non invasive method to inspect the large bowel. It enables to screen for colorectal polyps by way of images rendered from an endoluminal perspective. Polyps are well-known precursors to colon cancer. The size of a detected polyp is an important indication for diagnosis and decision making. It is generally accepted that polyps with a diameter smaller than 5mm require no direct further action, whereas polyps larger than 10mm should be removed. The policy with patients harboring polyps with a size between 5mm and 10mm is to have a follow-up CT-scan several years later. Unfortunately, current colonographic visualization techniques are still rather time consuming. More important, large polyps are sometimes missed. Therefore, methods have been proposed to support the inspection by way of computer aided diagnosis (CAD).. Like most CAD systems, automated polyp detection usually consist of three basic steps: (1) segmentation of the colon wall; (2) candidate generation and (3) supervised pattern recognition. A good approximation to the true colon wall (defining the region of interest) is obtained rather easily due to the large contrast between tissue and air/CO2 inside the colon. However, partial volume effects may affect the image intensity at thin colonic folds. Still, most techniques use a thresholding at a fixed value of around -650 Hu. Finding candidate objects on the colon surface is a much more challenging task. Summers et al. propose to use methods from differential geometry. a triangle mesh is extracted from 3D CT data after which principal curvatures were computed by fitting a 4th order b-spline to local neighborhoods with a 5 mm radius. Candidates were generated by selecting regions with a

positive1 mean curvature. Yoshida et al. use the shape index and curvedness to find candidate objects on the colon wall. The shape index and curvedness are functions of the principal curvatures K1 and K2:

$$SI = \frac{1}{2} - \frac{1}{\pi} arctan(\frac{\kappa_1 + \kappa_2}{\kappa_1 - \kappa_2}) \; and \; CV = \sqrt{\frac{\kappa_1^2 + \kappa_2^2}{2}}$$

and are computed using a Gaussian-shaped window (aperture). Alternatively, Kiss et al. generate candidates by searching for convex regions on the colon wall. Their method fits a sphere to the surface normal field. The side on which the center of the fitted sphere is found (in tissue or in air) determines the classification of the surface as convex or concave. Roughly 90% of the colon wall is classified as concave, that is as 'normal'. To the remaining part of the colon surface a generalized Hough transformation is applied using a spherical model. Candidate objects are generated by finding local maxima in the parameter space created by the Hough transformation. Simply selecting regions on the colon that protrude inwards yield too many candidates. Therefore, thresholds on mean curvature, principal curvatures, sphericity ratio and/or shape index are used as restrictive criteria. Unfortunately, their values are sensitive to e.g. the CT image noise level and the size of the local neighborhood used to compute them. Generally, the thresholds are set conservative in order not to harm the sensitivity. All of the above CAD schemes are based on the modelling of an approximately spherical polypoid shape, although, many polyps are often far from symmetric, let alone spherical. Therefore, the candidate generation step of these schemes is characterized by low specificity and much effort is needed to improve specificity while preserving a high sensitivity. The problems associated with modellingpolyps as spherical protrusions are presented in figure 1. It shows the (κ_1, κ_2)-space. The horizontal axis shows the first principal The vertical axis shows the second principal curvature, κ_2. Since the first principal curvature is by definition larger than or equal to the second ($\kappa_1 \geq \kappa_2$) all convex points on the colon lie inside the region given by $\kappa_2 > 0$ and $\kappa_1 \geq \kappa_2$. Points on perfectly spherical protrusions lie on the line $\kappa_1 = \kappa_2$ (SI = 1). On the other hand, perfect cylindrical folds lie on the line $\kappa_2 = 0$ (SI = 0.75). Objects with a larger radius yield smaller principal curvature values and therefore show up closer to the origin. Additionally larger polyps tend to be more asymmetric and therefore more fold-likewhen described by

the shape index. Both large and small polyps are found close to the borders defined by the thresholds on SI and CV as indicated in figure 4.1. As a consequence the criteria used to limit the numberof candidate detections are at least as stringent for the larger polyps as for the smaller ones. Notice that this behavior is in conflict with clinical decision making, which dictates that large polyps are more important than smaller ones, since the former have a larger probability to develop into colon cancer. To comply with clinical practice, one needs a candidate generation step steered by parameters that directly reflect polyp size, such that variations in thresholds only affect the CAD system's sensitivity for small polyps. In this paper, we introduce a method to estimate the physiological, background shape of the colon wall. Polyp candidates are detected as a local deviation from the background. Our method locally flattens/deforms the colon wall in order to 'remove' the protrusions. The amount of displacement needed for this deformation is used as a measure of 'protrudness' of the underlying lesion. Regions where this measure has a high value are considered as candidate polyps, after which the protrusion measure together with a few additional features is used in supervised pattern recognition

figure 1: left: t four thick lines enclose a region in the (κ 1, κ 2)-space. the curved lines represent thresholds on the curvedness, while the straight lines enclose the region given by 0.9 < si ≤ 1. the center image shows the κ 1 and κ 2 values as measured on candidate objects. (see results section) the light grey objects are false positives. the circles are tp that have a largest shape index of at least 0.9. the black squares represent tp as wel but have a largest shape index smaller than 0.9. the right image shows a typical polyp shape.

2. METHOD

A typical polypoid shape is shown in Figure1(right). Suppose that the points on convex parts of the polyp (the polyp head) are iteratively moved inwards. In effect this will 'flatten' the object. At a certain amount of deformation the surface flattening is such that the complete protrusion is removed. That is, the surface looks like as if the object was never there. This is the key concept on which the method is based. A more formal presentation follows from the description of the surface shape using the principal curvatures. Protrusions are

defined as those regions on the surface where the second principal curvature is larger than zero (This implies of course that the first and largest principal curvature is larger than zero as well). The method then deforms the surface until the second principal curvature is smaller or equal to zero. Clearly, this will only affect structures that are curved in two directions like polyps and will not deform curved structures like folds. Folds typically bend in one direction only and have a first principal curvature larger than zero and a second principal curvature around zero. Figure.1 illustrates how polyps modelled as spherical mounds are found near the line κ 1 = κ 2 with κ 2 > 0. From here on we drop the spherical model and note that polyp 'heads' are characterized by a κ 2 > 0. Consequently all regions on the colon wall where κ 2 > 0 are considered as candidate objects. The requirement κ 2 > 0 is less strict than used in most other state of the art systems, which put restrictions on the curvature values. For example by limiting the allowed shape index values to: SI > 0.8. One might argue that this will lead to many more candidates. This is unarguably true. We will show, however, that the proposed method does not require any thresholds other than

κ 2 > 0. Moreover, the deformation method described below leads to a quantitative measure of the polyp protrudness and therefore permits ordering of the generated candidate objects in a way intuitive to the radiologist. In effect this will reduce the number of candidates that are passed to the classification.

. **1.1 Surface Evaluation**

The method employs surface evolution on triangle meshes The triangle mesh is generated by the marching cubes algorithm applied to the 3D CT data using a threshold of -750 Hu. A typical mesh size consist of around 106 vertices. method was presented to rapidly remove rough features (noise) from irregularly triangulated data. It was based on the diffusion equationAn important aspect that is used in deciding on a patient's treatment is the polyp size. It is measured from the largest object diameter in cross sectional views or in volume renderings . A role of CT colonography in screening is to pre-select patients with polyps such that only patients with polyps are sent to colonoscopy. Another advantage of CT colonography that it aids colonoscopy by localizing the lesion and hence increasing the overall sensitivity.

$$\frac{\partial X_i}{\partial t} = \lambda L(X_i), \text{ with } L(X_i) = \left(\frac{1}{N_1}\sum_{j \in 1ring} X_j\right) - X_i$$

.

where L(Xi) is a discrete (1-ring) estimate of the Laplacian at vertex i. X are the positions of the mesh points, N1 is the number of vertices in the 1-ring neighborhood of vertex Xi and λ is the diffusion coefficient. The solution at time t was
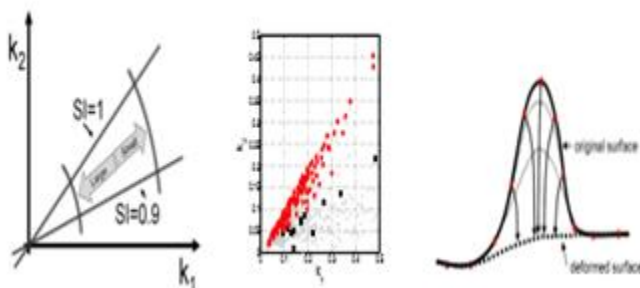
found using a backward Euler method which translated the problem into a matrix-vector equation

$$(\mathbf{I} - \lambda\, dt\mathbf{L})\bar{X}^{t+1} = \bar{X}^t$$

The matrix M = I−λdtL is sparse and its structure is given by the mesh one-ring relations, ⁻X is a vector containing all mesh points and I is the identity matrix. This system can be solved efficiently using the bi-conjugate gradient method [91]. In [24] the diffusion was applied to all mesh points. A well known effect of prolonged diffusion on the complete mesh is global mesh shrinking and   solution was proposed by compensating for the reduction of the mesh volume. We, however, apply the diffusion only to a limited number of mesh points, namely the points where κ 2 > 0. The majority of points have negative or zero second principal curvature and remain at their original position. They provide the boundary conditions for the other points. Therefore, in contrast to the method suggested global shrinking is not an issue and we can search for the steady state solution of the diffusion equation

$$\frac{\partial X_i}{\partial t} = L(X_i) = 0$$

The discrete Laplacian estimates the new position of vertex Xi by a linear combination of its 1-ring neighbours, Xj. Rewriting equation 4.4 then yields a matrix-vector equation

$$\left(\frac{1}{N_1}\sum_{j\in 1ring\, i} X_j\right) - X_i = \mathbf{M}\bar{X} = 0$$

Fortunately, M is sparse and its structure is given by the 1-ring mesh relations. The number of non-zero elements on each row equals the number of 1-ring member vertices. Like the backward Euler formulation this equation can also be solved efficiently using the bi-conjugate gradient method [91]. It is well known that the solution to the Laplace equation minimizes the membrane energy subject to the imposed boundary conditions. However, our objective is not to minimize the mean curvature, but to minimize the second principal curvature. Therefore, we extend the above equation by introducing a 'force' term. The resulting equation is a Poisson equation

$$L(\bar{X}) = \bar{F}(\kappa_2)$$

This equation reads as follows: the new positions of the mesh points are found by initially moving each mesh vertex to a position as prescribed by the Laplacian operator.

Subsequently, the term on the right hand side 'pushes back' the point such that the resulting second principal curvature is zero. The force term ⁻F is designed to depend on κ 2 and is updated after solving equation 4.6. In other words we solve iteratively. The force term is initialized with ⁻L(X) such that we start wit

$$\bar{F}^{t=0} = L(\bar{X})$$

Thus, the 'force field' ⁻F initially balances the displacement prescribed by the Laplacian and leaves the mesh unaltered. After each iteration ⁻F is updated with

$$\bar{F}^{t+1} = \bar{F}^t - \kappa_2^t \frac{A_{1ring}}{2\pi}\bar{n}$$

where A1ring is the surface area of the 1-ring neighborhood and ⁻n is the vertex normal. The last term can be interpreted as a correction term. Note that if κ 2 is positive k⁻Fk should be relaxed. On the other hand, the magnitude of the reduction term additionally depends on the sampling density of the mesh. If the sampling is dense and A1−ring small the magnitude of the correction term should be small. Since κ 2 equals the reciprocal of the radius of the surface tangent circle (R = 1 κ 2) in κ 2-direction, the term 2 π κ 2 2 is half of the area of the fitting sphere. Therefore, the displacement R needed to remove the curvature in second principal direction is normalized by the ratio of these two areas. The estimated displacement is given by

$$d_{est} = R\frac{A_{1ring}}{2\pi/\kappa_2^2} = \kappa_2\frac{A_{1ring}}{2\pi}$$

The resulting displacement of the mesh points yields a deformed mesh which is an estimate of how the colon wall looks like in the absence of protrusions. The amount of displacement of each mesh point (e.g. in millimeters) is a quantitative measure of the 'protrudness'. Candidate objects are generated by applying a threshold on the displacement field.

3.RESULTS

The performance of the method was tested using clinical data from a large, previous study . Automatic polyp detection was executed in three steps: (1) segmentation of the colon wall via the marching cubes algorithm; (2) candidate generation using protrudness; (3) supervised pattern recognition involving a linear classifier and only a few featurespartially covered by (bright) fluid, which hampers its detection. In such situations, digital techniques are required to

3.1 Experimental Data

A total of 249 consecutive patients at increased risk for colorectal cancer were included in a previous study [123]. These patients underwent CT colonography before colonoscopy, which served as the gold standard. All patients were scanned in both prone and supine position. The size of a polyp identified during CT colonography was measured in reformatted images, in which the largest polyp diameter was selected for size measurement. Polyp size was also measured during colonoscopy by comparison with an open biopsy forceps of known size. The colonoscopy findings were matched with the CT data. 13 patients were selected that contain 1/3 of the polyps larger than 5 mm from the complete study. This yielded 64 polyps larger than 5 mm. 34 of 64 polyps could be identified in both the prone and the supine CT scan and 30 were identified on either scan but not on the other. Consequently, there were 98 example objects in total. Figure 4.4 (left) shows a histogram of the CT size-measurements. The majority of objects have a size between 5 and 7 mm. 42 are smaller than 5 mm and are considered as clinically unimportant. 28 are in the range [5,6]mm, 63 are in the range (6,10]mm and 32 are larger than 10mm
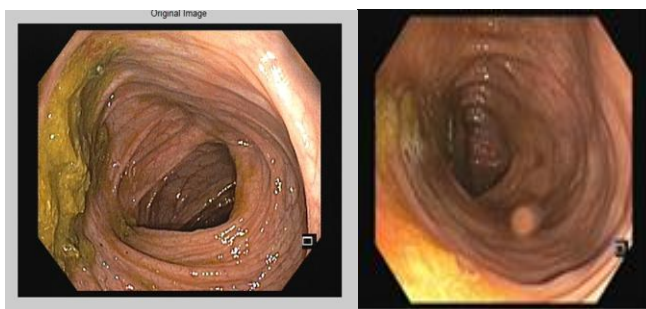

Fig 2. Database

3.2. Candidate Generation:

A typical result is given in figure 4.2. It shows three renderings of the colon wall surface. In the left picture an isosurface volume rendering of a 7 mm large polyp is shown. The polyp is situated on a folded colon structure. The middle picture shows the deformed mesh (visualized by a mesh rendering). The protrusion is 'removed', demonstrating how the colon may have looked like in the absence of the polyp. The right image shows the original mesh with the segmentation obtained by thresholding the protrusion measure at a value of 0.1mm An other example is presented in figure 4.3. The left picture shows an isosurface volume rendering. In the center of the picture a large (14mm) non-spherical polyp is situated between two folds. The middle picture shows the segmentation as obtained by hysteresis thresholding the shape index using values 0.8 and 0.9 and curvedness values in the range: 0.05<CV<0.25. The same thresholds were used to generate
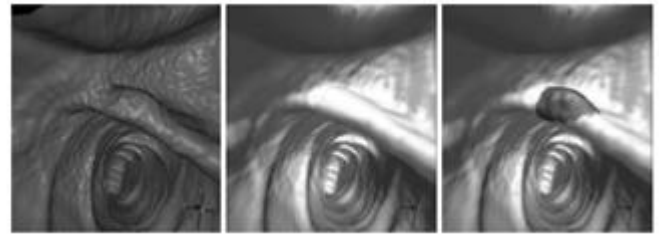

Figure 3: Example of the deformation applied to a polyp on a fold. Left: the original colon surface with a polyp on a fold (isosurface volume rendering). Middle: the deformed surface mesh with the polyp 'removed' (mesh rendering). Right: the obtained segmentation by thresholding the displacement field (mesh rendering).

candidate objects. The shape index and curvedness were computed by fitting a 2nd order polynomial to the mesh using a local neighborhood with 5mm radius. Due to the irregularity of the protrusion several segments of the polyp have been found. The right picture shows the segmentation as a result of thresholding the protrusion measure (value 0.1mm). A more coherent segmentation has been obtained. Our method applied to the 13 patients yielded 1578 candidate objects (including the true positives), which is ±60 per dataset. A total of 3 polyps (between 5mm and 6mm) were missed in the candidate generation step. In contrast, if a threshold of 0.9 on the shape index was used to segmented candidates a total of 16 polyps would have been missed. (See figure 4.1 (middle)). From the segmented candidates the vertex with largest shape index value was found. For this vertex the $\kappa 1$ and $\kappa 2$ values are plotted in figure 4.1 (middle). This plot does not include the 3 missed polyps.

3.3 CAD Performance:

The candidate generation step was used as an input to supervised pattern recognition. In figure 4.4 we show ROC curves based on a linear classifier applied to four features: the maximum protrusion found on a candidate object; the size of the object measured as proposed in [26]; volume, obtained from the enclosed volume between the original mesh and the deformed mesh and the percentage of SI values for the vertices on the segmented surface patch, that is within the range of 0.65 < SI < 0.85. The latter value is expected to attain high values on folded structures. Three lines in figure 4.4 (right) show the performance of the system for different size classes. The data was generated in a leave-one-patient out manner. The large polyps (>10mm) are found with 100% sensitivity at a FP rate of 13 per dataset and 90% sensitivity at 2 FP per dataset. The ROC for polyps larger than 6 mm (including those larger than 10mm) show that 80% sensitivity is obtained at the cost of 4 FP per dataset. A 95% sensitivity is obtained at the cost of 10 FP per dataset. The results for polyps larger than 5mm are similar to the results for polyps larger than 6mm. However, 100% sensitivity is not reached This is due to the fact that in the candidate generation step 3 polyps between 5mm and 6mm have been

missed. The plots in figure 4.4 demonstrate that the specificity of the CAD system is even higher if the sole purpose of the system is for diagnostic purposes only, namely to decide whether a patient has or has not any polyps. The left plot shows how many false positives have been assigned a higher posterior probability than the first large polyp (>=10mm). It follows that for 7 out of 13 patients the first object is a polyp. For one patient three false positives have a higher posterior probability than the first polyp. Note that the total number of patients is 11 (and not 13). This is due to the fact that 2 patients did not have polyps larger than 10mm. The right plot shows the number of false positives with a higher posterior probability than any of the polyps larger than 6mm (including those larger than 10mm). Note that including the smaller polyps improves the results. Apparently some of the small polyps are assigned a higher posterior probability than the large one
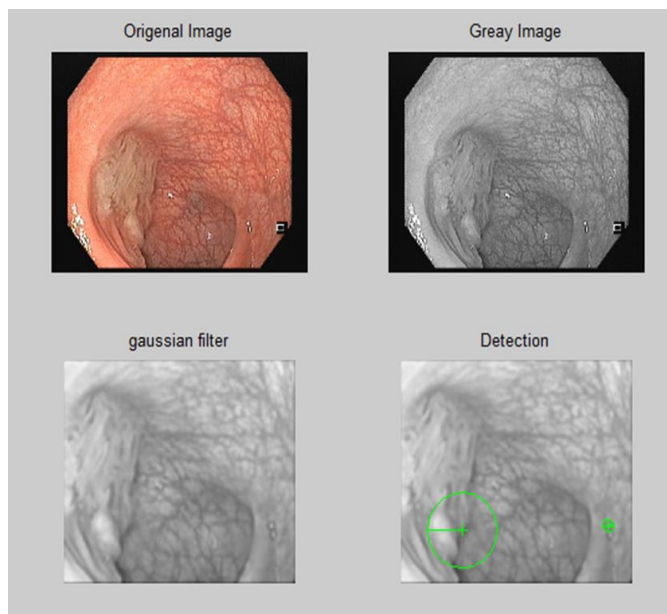

Fig4: final results with green circle indicates polyp detection

4.CONCLUSION

We have presented a method to detect protruding objects on curved surfaces. It was used to generate candidate objects for automated polyp detection. The method works by locally flattening the colon wall in order to 'remove' protrusions. Actually, the colon surface is deformed until the second principal curvature is smaller than or equal to zero. Therefore, only those structures are affected that are curved in two directions, like polyps. Folds remain unaltered. The amount of displacement needed for flattening/deformation is used as a measure of 'protrudness' of the object. A threshold on the deformation field is the only parameter needed for candidate generation. This is a clear advantage over methods that involve many restriction criteria. Another advantage is

that the deformation field immediately allows for the computation of additional features such as the object's volume. We have shown that a simple linear classifier involving only four features already yields 95% sensitivity at the cost of about 10 FP per dataset. Clearly, the algorithm must be extensively tested. We do realize an investigation on more data involving more complex classifiers is needed to be conclusive on the overall improvement of polyp detection. However, the current results give an indication that the protrusion measure may enhance polyp detection scheme

References

[1] D. G. Adler and C. J. Gostout, "Wireless capsule endoscopy," Hospital Physician, vol. 39, pp. 14–22, 2003., Germany: Springer, 1989, vol. 61.

[2] L. Breiman, "Random forests," Mach. Learn., vol. 45, pp. 5–32, 2001..

[3] A. Buades, T. Le, J.-M. Morel, and L. Vese, Cartoon+texture image decomposition, image processing on line 2011 [Online]. Available: http://dx.doi.org/10.5201/ipol.2011.blmv_ct R. E. Sorace, V. S.

[4] Reinhardt, and S. A. Vaughn, "High-speed digital-to-RF converter," U.S. Patent 5 668 842, Sept. 16, 1997.

[5] Y. Cao, D. Li, W. Tavanapong, J. Oh, J. Wong, and P. C. De Groen, "Parsing and browsing tools for colonoscopy videos," in Proc. 12th Annu. ACM Int. Conf. Multimedia, 2004, pp. 844–851, ACM M. Shell. (2002) IEEEtran homepage on CTAN. [Online]. Available: http://www.ctan.org/tex-archive/macros/latex/contrib/supported/IEEEtran/

[6] FLEXChip Signal Processor (MC68175/D), Motorola, 1996 Y. Cao, D. Liu, W. Tavanapong, J.Wong, J.H. Oh, and P.C. DeGroen, "Computer-aided detection of diagnostic and therapeutic operations in colonoscopy videos," IEEE Trans. Biomed. Eng., vol. 54, no. 7, pp. 1268–1279, Jul. 2007.

[7] F. Condessa and J. Bioucas-Dias, "Segmentation and detection of colorectal polyps using local polynomial approximation," in Image Analysis and Recognition. New York: Springer, 2012, pp. 188–197A. Karnik, "Performance of TCP congestion control with rate feedback: TCP/ABR and rate adaptive TCP/IP," M. Eng. thesis, Indian Institute of Science, Bangalore, India, Jan. 1999.

[8] C. Cortes and V. Vapnik, "Support-vector networks," Mach. Learn., vol. 20, pp. 273–297, 1995.

[9] Wireless LAN Medium Access Control (MAC) and Physical Layer (PHY) Specification, IEEE Std. 802.11, 1997 M. Delvaux and G. Gay, "Capsule endoscopy: Technique and indications," Best Practice Res. Clin. Gastroenterol., vol. 22, pp. 813–837, 2008

[10] .R. Eliakim, "Video capsule colonoscopy:Where will we be in 2015?," Gastroenterology R. Eliakim, "Video capsule colonoscopy:Where will we be in 2015?," Gastroenterology vol. 139, 2010, p. 1468.

[11] .] R. Eliakim, K. Yassin, Y. Niv, Y. Metzger, J. Lachter, E. Gal, B. Sapoznikov, F. Konikoff, G. Leichtmann, Z. Fireman, Y. Kopelman, and S. Adler, "Prospective multicenter performance evaluation of the second-generation colon capsule compared with colonoscopy," Endoscopy, vol. 41, pp. 1026–1031, 2009.

[12]   P.Figueiredo,I.Figueiredo,S.Prasath,andR.Tsai,"Automati cpolyp detection in pillcam colon 2 capsule images and videos: Preliminary J.Gerber ,A. Bergwerk,andD.Fleischer,"A capsule endoscopy guide for the practicing clinician: Technology and troubleshooting," Gas- trointestinalEndoscopy, vol. 66, pp. 1188–1195, 2007. feasibility report," Diagnostic Therapeutic Endoscopy, p. 182435, 2011

[13]   J.Gerber,A.Bergwerk,andD.Fleischer,"Acapsuleendoscop yguide for the practicing clinician: Technology and troubleshooting," Gas- trointestinalEndoscopy, vol. 66, pp. 1188–1195, 2007.

[14]   B. Gustafsson, H.-O. Kreiss, and J. Oliger,TimeDependentProblems andDifferenceMethods,PureandAppliedMathematics. NewYork: Wiley, 1995

[15]   . R.M.HaralickandL.G.Shapiro,ComputerandRobotVision. New York: Addison Wesley, 1992, vol. I, pp. 28–48.